

WHAT IS THE SPATIAL RELATIONSHIP BETWEEN HARD X-RAY FOOTPOINTS AND VERTICAL ELECTRIC CURRENTS IN SOLAR FLARES?

JING LI, THOMAS R. METCALF,¹ RICHARD C. CANFIELD,² AND JEAN-PIERRE WÜLSER¹
Institute for Astronomy, University of Hawaii, 2680 Woodlawn Drive, Honolulu, HI 96822, U.S.A.

AND

TAKEO KOSUGI

National Astronomical Observatory of Japan, Mitaka, Tokyo 181, Japan

Received 1996 September 18; accepted 1997 January 13

ABSTRACT

We examine the spatial relationship between solar hard X-ray sources observed with the Hard X-Ray Telescope aboard *Yohkoh* and photospheric electric currents observed at Mees Solar Observatory. In 1993, Canfield et al. concluded that energetic electron precipitation tends to occur at the edge of sites of high vertical current. They did not, however, have a direct diagnostic of particle precipitation; they used H α Stark-wing emission as a proxy. In this paper, we analyze hard X-ray images and vector magnetograms of six flares of M/X X-ray class to reach two basic conclusions. First, we confirm that electron precipitation avoids sites of high vertical current density at photospheric levels, preferentially occurring adjacent to these current channels. Hence, we conclude that our observations rule out flare models in which nonthermal electrons are accelerated within the large-scale active-region current systems that are observed by present vector magnetographs. Second, at conjugate magnetic footpoints the stronger hard X-ray emission is associated with smaller vertical current density and weaker magnetic field. This result is consistent with a “cornucopia”-shaped magnetic morphology in which precipitating electrons are preferentially deflected away from the narrower footpoint by magnetic mirroring.

Subject headings: MHD — Sun: flares — Sun: X-rays, gamma rays

1. INTRODUCTION

It is generally accepted that the relaxation of a non-potential magnetic field configuration powers solar flares. A complete understanding of how the magnetic energy is released is still lacking, however. In this paper we study the morphological relationship between solar flare sites of energetic electron precipitation, observed in hard X-rays, and electric current distribution observed at the photosphere. The energetic electrons precipitate onto the atmosphere along the magnetic fields and are responsible for the hard X-ray production. Therefore, the relationship between the hard X-rays and the electric currents will help us understand how the magnetic free energy is released as energetic particles precipitating onto the dense chromosphere to produce hard X-rays.

In previous studies, H α flares were used as an indirect observation of electron precipitation onto the solar atmosphere, since direct hard X-ray observations were not available. Moreton & Severny (1968) studied 30 flares and found that $\sim 80\%$ of the initial brightenings in H α were coincident with the sites of vertical currents, to within the 6'' co-alignment accuracy of their data. Hagyard (1984) studied a single flare and found that bright regions in H α were located near the principal current system. The sites of strongest H α emission were found to be cospatial with the vertical current systems, to within the 2'' registration accuracy by Lin & Gaizauskas (1987). Further study revealed that the strongest flares were closely associated with vertical currents. Some of the flares were cospatial with current maxima, but most appeared near the edges of currents and

occasionally between current channels of opposite sign (Romanov & Tsap 1990).

These studies, based on observations of currents from vector magnetograms, concluded that their observations support the current-interruption model of flares (Alfvén & Carlqvist 1967; Smith & Priest 1972; Spicer 1981). These authors had in mind the interruption of the currents revealed in their observations, i.e., large-scale active-region current systems. However, other studies have reached a different conclusion, largely on the basis of simple longitudinal magnetic field observations. The difference between these conclusions and the ones based on vector magnetograms is fundamental. The former studies have examined the role of active region magnetic *topology* in flares, considering the role of magnetic separators and separatrixes (Baum & Bratenahl 1980; Gorbachev & Somov 1988; Démoulin et al. 1994). These topological features are defined directly by the boundaries between flux systems and only indirectly by the flux systems themselves (e.g., large-scale active-region current systems). Observational studies of flares and magnetic field topology (Machado et al. 1983; Mandrini et al. 1995; Démoulin et al. 1993; Brown et al. 1994; Bagalá et al. 1995) have concluded that flares tend to occur at locations near separatrixes and separators.

More recent observational work of the type based on vector magnetograms has examined the relationship of flare features in H α spectroheliograms, as opposed to H α filtergrams, to the large-scale currents. In the absence of hard X-ray data, Stark wings in H α spectral images were used to identify the electron precipitation sites at the chromosphere (Canfield et al. 1993). Studies of several flares (Leka et al. 1993; de La Beaujardière, Canfield, & Leka 1993) confirmed that sites of intense nonthermal electron precipitation do not overlap regions of strong vertical current at the photosphere. They concluded that the energetic electron

¹ Now at Lockheed Martin Advanced Technology Center, Department H1-12, Building 252, 3251 Hanover Street, Palo Alto, CA 94304.

² Now at Department of Physics, Montana State University, Bozeman, MT 59717-0350.

precipitation sites tend to occur on the shoulders of channels of high vertical current density rather than at the vertical current density maxima.

In this paper, energetic electron precipitation sites are determined from *Yohkoh* Hard X-Ray Telescope (HXT; Kosugi et al. 1991) images of six intense flares. This direct observation of the hard X-ray emission is an important improvement over previous studies, in which H α was used as a proxy. The vertical current density maps at the photosphere are calculated from magnetograms observed with the Haleakala Stokes Polarimeter at Mees Solar Observatory (MSO). The morphology of the magnetic field in the corona is inferred from images made with the *Yohkoh* Soft X-Ray Telescope (SXT; Tsuneta et al. 1991).

2. OBSERVATION AND ANALYSIS METHODS

The photospheric vertical currents are calculated from Fe I 6301 Å and 6302 Å vector magnetograms obtained by the Haleakala Stokes Polarimeter (Mickey 1985) at MSO. The magnetic field calibration of this instrument is described in detail by Canfield et al. (1993). Both high (2".8 per pixel) and low (5".6 per pixel) spatial resolution magnetograms are used for our study. We find no evidence that either the spatial resolution or the stability of imaging during the observations have a significant effect on the locations of currents that we infer (Gary & Démoulin 1995). The 180° ambiguity in the measurement of the transverse fields is resolved with the "minimum energy" algorithm (Metcalf 1994).

The HXT is a Fourier synthesis imager consisting of 64 bi-grid modulation collimators. It provides simultaneous imaging in four energy channels, LO (13.9–22.7 keV), M1 (22.7–32.7 keV), M2 (32.7–52.7 keV), and H (52.7–92.8 keV). The temporal resolution of the flare mode is 0.5 s (Kosugi et al. 1991, 1995). We used a pixon-based multiresolution image reconstruction technique (Metcalf et al. 1996) in each energy channel to generate images. For the flares studied, each image contains a maximum of 64 × 64 pixels, with each pixel corresponding to 2".46.

To study the spatial relationship between flare hard X-ray sites and sites of vertical current, we chose flares according to three criteria:

1. The integral photon count of hard X-rays should be greater than 150 counts per subcollimator in the H band (53–93 keV), so that the X-ray flux provides enough information for the synthesis of images.
2. Vector magnetograms corresponding to the flaring active regions must be observed within 12 hr of the flare by the Stokes Polarimeter at MSO, so that current maps can be constructed from magnetograms without major effects due to active region evolution.
3. The active regions should be within about 45° of the center of the disk, so that vertical current distributions are not seriously distorted by projection effects (Gary & Hagyard 1990).

The co-alignment between hard X-ray images and magnetograms is important for our study. As HXT does not have white-light images of active regions, the co-alignment is performed with white-light images from the Soft X-Ray Telescope on board *Yohkoh*. The SXT white-light images were aligned with continuum images from the Haleakala Stokes Polarimeter. Since the alignment between SXT and HXT is known (Masuda et al. 1995), we can then align the

HXT images with the magnetograms. After 1993, SXT no longer provided white-light images. For these data, the co-alignment was performed with full-disk white-light images from Mees Solar Observatory, which were referenced to the SXT and HXT image coordinates. The accuracy of the alignment was about 4" for the data from 1991, 1992, and 1994, and about 6" for the data from 1993. The 1993 co-alignment is less accurate since the Mees White Light Telescope did not have optimal spatial resolution; in 1994 it was upgraded. The Sun's rotation is appropriately removed for the alignment between HXT observations and Haleakala Stokes Polarimeter observations.

Our study uses four different types of observations:

1. Hard X-ray light curves in the four HXT energy channels (Kosugi et al. 1995) provide the burst spectrum and its fluctuation with time. On the basis of the light curves, we reconstruct images for each major hard X-ray burst (spike) using appropriate integration periods.

2. Soft X-ray images clarify the morphology of the magnetic field in the corona and provide a check on the synthesis of the HXT images. We use SXT movies taken with the Al.1 filter to help identify conjugate magnetic footpoints. Since the SXT images with the Be119 filter reflect the very hot plasma (Hara et al. 1994), and reflect the same primarily-thermal emission seen in the HXT LO energy channel, we use them to check the HXT image reconstruction.

3. In the thick-target model (Brown 1971), hard X-ray images of flares on the solar disk identify sites of particle precipitation into the lower atmosphere (in contrast to limb flares, in which the footpoints are obscured; Masuda et al. 1994). Images in the high-energy channels M2 and H unambiguously reflect the presence of nonthermal electrons. Footpoint hard X-ray intensities (counts pixel⁻¹ s⁻¹) are compared with the cospatial magnetic flux and vertical current density observations.

4. Haleakala Stokes Polarimeter vector magnetograms indicate the magnetic field strength and vertical current density in the particle precipitation sites. The co-aligned hard X-ray images and current density maps show their morphological relationship at the photosphere.

3. OBSERVATIONS

We studied the six *Yohkoh* flares listed in Table 1, which satisfy our selection criteria. In addition to the usual flare descriptors, the table distinguishes between the times of the hard X-ray flares and accompanying magnetograms. As a rule, we do not expect these time differences to be significant, in view of the observed active region evolution and our spatial resolution. The most likely exception is the flare of 1992 August 20. This event occurred in AR 7260; the rapid development of this active region, due to flux emergence, is well known (Leka et al. 1994). The table also lists the estimated uncertainty (σ) of the vertical current density J_z measurements as inferred from regions of no significant transverse field. We consider features with $J_z > 3 \sigma$ reliable, though even 1.5 σ may reflect something real.

3.1. 1991 November 15

This flare, at approximately 22:37 UT, has been studied extensively (Canfield et al. 1992; Sakao et al. 1992; Wülser et al. 1994; see also Hara et al. 1992 for AR 6919 observations). The hard X-ray light curves show three

TABLE 1
SUMMARY OF SIX FLARE EVENTS

NOAA Region	UT Date	Location	X-Ray Class ^a	H α Importance	UT (Hard X-Ray) ^b	UT (J_z) ^c	σ (J_z) ^d
6919.....	1991 Nov 1	S13° W19°	X1.5	3B	22:37:50	23:46:00	3.41
6985.....	1991 Dec 26	S16° E23°	M4.2	1B	21:36:57	19:21:00	1.86
7260.....	1992 Aug 20	N16° W27°	M2.9	1B	09:04:30	00:52:00	3.61
7518.....	1993 Jun 07	S09° W30°	M5.4	2B	14:21:20	16:39:00	2.32
7530.....	1993 Jul 04	S11° W45°	M1.6	1B	07:48:40	17:06:00	3.09
7765.....	1994 Aug 14	S12° W08°	M3.9	1N	17:35:58	16:32:00	1.00

^a GOES X-ray class.

^b Peak times in HXT H channel.

^c Beginning times of the ~ 1 hr scan.

^d In units of mA m⁻².

spikes (called P1, P2, and P3 by Sakao et al. 1992). The preimpulsive phase A1.1 SXT image in Figure 1 (*left*) shows a loop system, brightest near its ends, which connects footpoints labeled “N” and “S.” The N and S features are $\sim 5''$ away from the vertical-field polarity inversion line, but much farther apart along it, implying that they are the footpoints of a highly sheared loop system. The soft X-ray image using the Be119 filter shows a bright area only at site N.

Hard X-rays and currents.—Figure 1 includes the HXT hard X-ray synthesized image in the H channel during P2 overlain by the vertical current density map. The HXT footpoint S appears to be right on the magnetic inversion line, another indication of the high shear of the magnetic field in this region. Canfield et al. (1992) compared the HXT M1 image with the vertical current distribution. They concluded that the S footpoint is at the edge of a region of significant vertical current density. We confirm this but note that the peak of the weaker hard X-ray source is separated from the peak vertical current density at footpoint S by an amount that is not significantly greater than the uncertainty of the co-alignment. On the other hand, it is unquestionable that the N footpoint is not at a region of significant current density. Both these attributes apply equally well to the P1

and P3 images, although the footpoint locations show systematic changes with time (Sakao et al. 1992).

Footpoint relationships.—In the burst shown, footpoint N showed strong hard X-ray emission (55 counts pixel⁻¹ s⁻¹), modest magnetic field strength (400 G), and insignificant vertical current density. Footpoint S showed weaker hard X-ray production (25 counts pixel⁻¹ s⁻¹), stronger magnetic field (800 G), and occurred in the vicinity of significant vertical current density. Therefore, the stronger hard X-ray source occurs at the magnetic footpoint having weaker magnetic field and insignificant vertical current.

3.2. 1991 December 26

This flare, at approximately 21:37 UT, had two peaks (which we call P1 and P2) in the HXT LO channel but only one in M1 and above. In Figure 2, evidence of two loop systems can be seen. One of the loop systems, roughly perpendicular to the magnetic neutral line, has conjugate footpoints in N and the east part of the bright beltlike area S. As well, the SXT A1.1 movie shows that the west part of S consists of footpoints of another system of loops whose conjugate footpoints fall in the bright circlelike area N2.

Hard X-rays and currents.—During LO spike P1, area S does not emit significant hard X-rays; only N2 shows

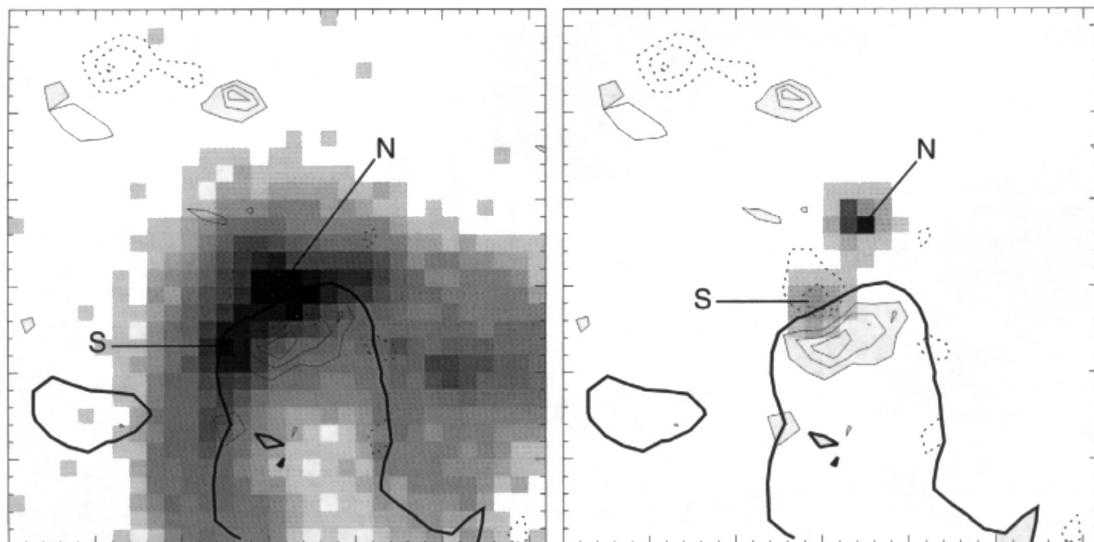


FIG. 1.—1991 November 15 flare. *Left*: Negative SXT image (Al.1 filter, 22:37:02), 31×31 pixels, each $2''.47$ square, overlain on magnetic field and currents data. *Right*: Negative HXT image (H channel, 22:37:32) during burst P2, integration period 22:37:32.6–22:37:39.6 UT. In Figs. 1–6, the thick solid contours indicate zero vertical magnetic field, the thin solid and dashed contours indicate 1.5, 3.0, 4.5, and 6.0 σ significance levels of J_z , the SXT and HXT image pairs have the same scale and orientation, and solar north is up, east to the left.

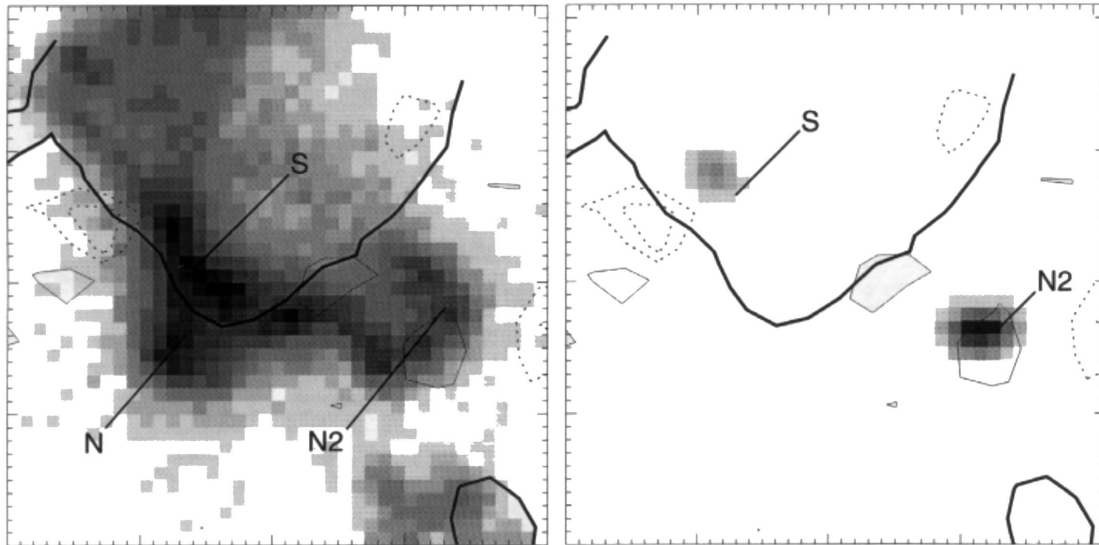


FIG. 2.—1991 December 26 flare. *Left*: SXT image (Al.1 filter, 21:36:42), 41×41 pixels, each $2''.47$ square. *Right*: HXT image (M2 channel, 21:37:41) during burst P2, integration period 21:37:41.9–21:37:49.9 UT.

strong emission. During P2, N2 brightens in all four HXT channels. The soft X-ray image with the Be119 filter shows brightening in the N2 and S areas during the flare. However, Figure 2 shows that M2 emissions occur in both areas S and N2 during P2. The S source is significantly displaced from any significant current. The N2 source is at the edge of a current at the 1.5σ level.

Footpoint relationships.—This flare clearly showed a double hard X-ray source. The hard X-ray intensity is 7.7 counts $\text{pixel}^{-1} \text{s}^{-1}$ in N2 and 1.7 counts $\text{pixel}^{-1} \text{s}^{-1}$ in S in the M2 channel. In the LO channel, S is consistent with the SXT image with the Be119 filter. The alignment shows that N2 has weaker vertical electric current density than the vicinity of S. The vertical magnetic flux is 200 G in N2 and 400 G in S. The stronger hard X-ray emission is coincident with the footpoint having weaker magnetic field and smaller nearby vertical current density.

3.3. 1992 August 20

Leka et al. (1994) showed that the following part of AR 7260, in which the flare of 09:04 UT occurred, was a complex magnetic δ configuration and was the site of vigorous flux emergence. The only available magnetogram was obtained 8.5 hr earlier than the flare, a possible problem. Two spikes, P1 and P2, are seen in the light curves of all four HXT channels. A long loop, connecting footpoints N and S, can be seen in the soft X-ray image in Figure 3.

The bright point N did not appear in the hard X-ray images. This is consistent with the SXT images taken with the Be119 filter.

Hard X-rays and currents.—In the M1 channel during spike P2, the hard X-ray image (Fig. 3) shows clearly that S consists of two bright hard X-ray sources (S1 and S2) and a fainter region A (Fig. 3). These three hard X-ray sites all are magnetic footpoints (as opposed to loop-top sources), since

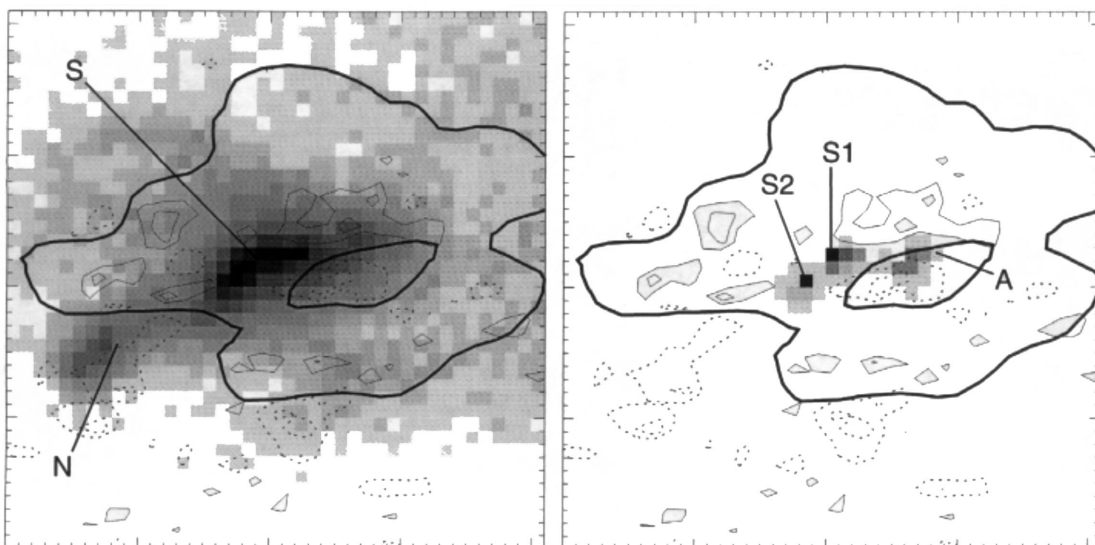


FIG. 3.—1992 August 20 flare. *Left*: SXT image (Al.1 filter, 09:03:57), 41×41 pixels, each $2''.47$ square. *Right*: HXT image (M1 channel, 09:04:19) during burst P2, integration period 14:20:57.8–14:21:42.8 UT.

a short soft X-ray loop extended from area A to the area S after the hard X-ray bursts. Figure 3 shows that the two hard X-ray sources, S1 and S2, avoid high vertical current density and high magnetic fields. The hard-ray source, A, is at the edge of a region of high current density, where the field strength is about 400 G.

Footpoint relationships.—This flare appears to have two double-footpoint sources, one associated with a loop connecting A with S1, another with a loop connecting A with S2. The stronger S1 and S2 footpoints each have a hard X-ray intensity ~ 2.5 counts pixel $^{-1}$ s $^{-1}$, while the weaker site A has 0.8 counts pixel $^{-1}$ s $^{-1}$, during P2 in the M2 channel. Figure 3 shows that the measured J_z values have the inverse relationship; only site A has a significant value of the measured vertical current density.

3.4. 1993 June 7

Before this M5.4 flare, at about 14:16 UT, the SXT A1.1 movie show a very large, complicated, and twisted loop system. The Be119 flare images, however, show that region N, as well as the portion of the loop parallel to the magnetic neutral line, is very bright throughout the flare. In the HXT M1 and M2 energy channels, three spikes (which we call P1, P2, and P3) are clearly seen; P2 is strongest (Kosugi et al. 1995). In all three spikes, the hard X-rays in the HXT LO channel show a looplike structure connecting the footpoints N and S. This feature is consistent with the Be119 SXT image.

Hard X-rays and currents.—During P1, the hard X-ray emission has two sources at N and one source at S in the HXT M1 and M2 channels. The hard X-ray production is stronger at N than at S. During P2 and P3 in the M1 to H channels, the hard X-ray burst has comparable strengths in both sites N (which is just a single source, see Fig. 4) and S. As Figure 4 shows, neither source coincides with regions of significant vertical current density, although both are close to regions that have marginally significant values.

Footpoint relationships.—This flare shows obvious hard X-ray double source structure. AR 7518, in which it occurred, had a pair of sunspots of comparable magnetic field strength, which is an unusually simple configuration in our data set. The hard X-ray double sources are near the

umbrae of this pair of spots. The hard X-ray brightness is stronger at footpoint N (10 counts pixel $^{-1}$ s $^{-1}$) than at footpoint S (6 counts pixel $^{-1}$ s $^{-1}$). The magnetic field strength is 1600 G in N and 3000 G in S. The maximum of the vertical current density is near S. The stronger hard X-ray emission occurs at the end of the loop that has notably weaker magnetic field.

3.5. 1993 July 4

The M1.6 flare of approximately 07:48 UT on this date had the weakest hard X-ray emission among the six flares we studied, though three spikes (which we call P1, P2, and P3) can still be seen clearly in the hard X-ray light curve in all but the H channel (Kosugi et al. 1995). There is no SXT observation of the flare area before the hard X-ray burst. Figure 5 shows the A1.1 soft X-ray image 30 s after the hard X-ray flare started. From the SXT movie, we can see twisted loops connecting the areas N and S.

Hard X-rays and currents.—The images synthesized from the HXT LO channel (14–23 keV) show a double source consisting of looplike emission structures near S and a much weaker source near N. This is consistent with the SXT Be119 image. In the HXT M1, M2, and H images, only source S is seen; it appears in all three spikes, including P2, which is shown in Figure 5. There is no significant vertical current at this location.

Footpoint relationships.—Site N has considerably stronger magnetic field strength (800 G) than the site S (200 G). Strong vertical currents are situated near footpoint N. The hard X-ray source is located in the end of a loop that has the weaker vertical magnetic fields and insignificant vertical current density.

3.6. 1994 August 14

The last of our six flares occurred at about 17:35 UT on this date. Two main spikes, P1 and P2, were seen in the M1, M2, and H channels of HXT (Kosugi et al. 1995). The SXT movie shows a large twisted loop with footpoints at S and N in Figure 6. A–N is the brightest portion of this large loop as seen through the A1.1 filter. The hard X-ray bursts occurred about 30 s after this image was taken. In the HXT

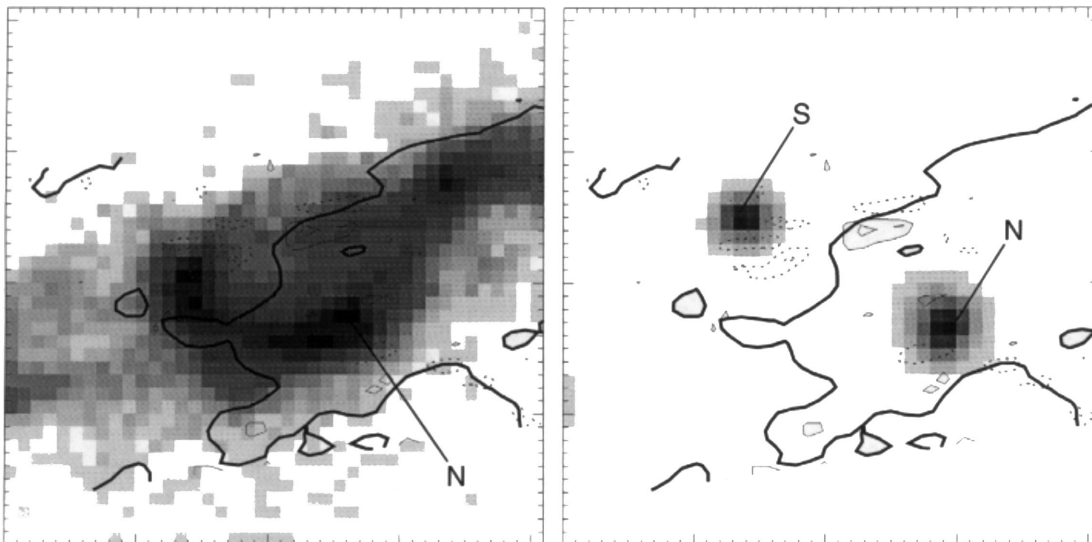


FIG. 4.—1993 June 7 flare. *Left*: SXT image (A1.1 filter, 14:15:56), 41×41 pixels, each $2''.47$ square. *Right*: HXT image (M2 channel, 14:20:57) during burst P2, integration period 09:04:19.6–09:04:40.6 UT.

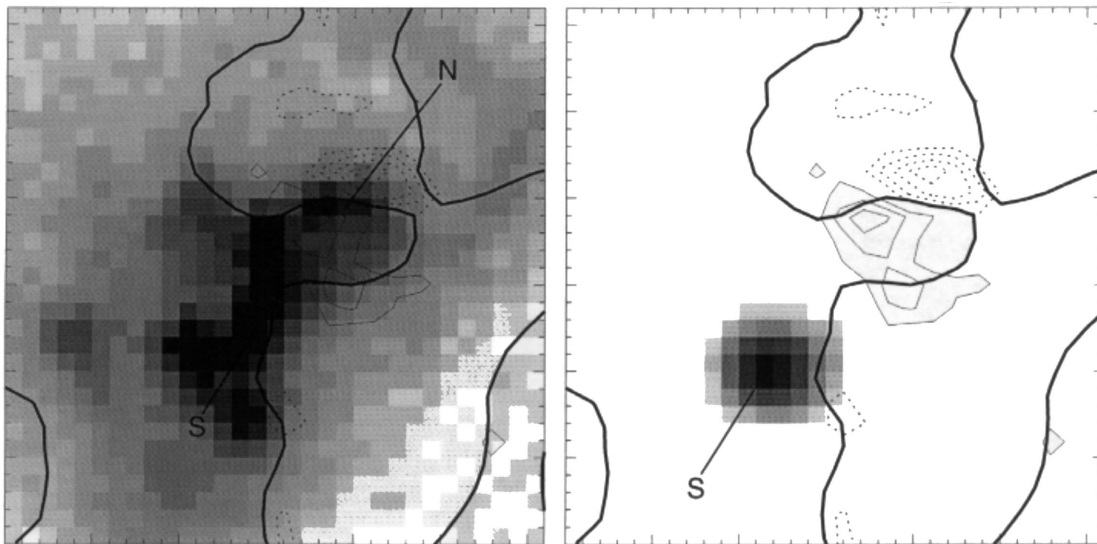


FIG. 5.—1993 July 4 flare. *Left*: SXT image (Al.1 filter, 07:48:28), 31×31 pixels, each $2''.47$ square. *Right*: HXT image (M1 channel, 07:48:31) during burst P2, integration period 07:48:31.1–07:48:59.1 UT.

LO channel, the images indicate similar patterns to the Be119 SXT images during both spikes P1 and P2.

Hard X-rays and currents.—Two hard X-ray footpoints are seen in the H-channel image during P1, the stronger burst (Fig. 6). Neither of them coincides with a current density maximum; both appear in on the shoulders of J_z peaks, at the lowest contour level. The weaker hard X-ray source at N is separated from the maximum vertical current density by about $10''$, a factor of approximately 2 greater than the uncertainty of coregistration of these data.

Footpoint relationships.—In the image during spike P1 (Fig. 6), site S ($2.2 \text{ counts pixel}^{-1} \text{ s}^{-1}$) is brighter than N ($1.3 \text{ counts pixel}^{-1} \text{ s}^{-1}$). In the corresponding image during the weaker spike P2, the two sites are comparable. The magnetic field strength is 800 G at site N and 400 G at site S. The highest value of J_z is next to site N. Hence, the weaker

hard X-ray emission is associated with higher vertical current density and stronger magnetic field.

4. DISCUSSION

All but one of the events we have studied have more than one hard X-ray feature. We have determined the hard X-ray brightness of each footpoint source by integrating over it, after background subtraction. The relationship between hard X-ray footpoint brightness, magnetic field strength, and vertical current density is consistent in our data set.

The stronger hard X-ray emission always occurs at the footpoint having relatively weaker magnetic field (Table 2). This independently confirms the finding by Sakao (Sakao 1994; see also a review by Kosugi 1996), since his data set and ours have only one event in common. Figure 7 cartoons the “cornucopia” magnetic geometry that most simply

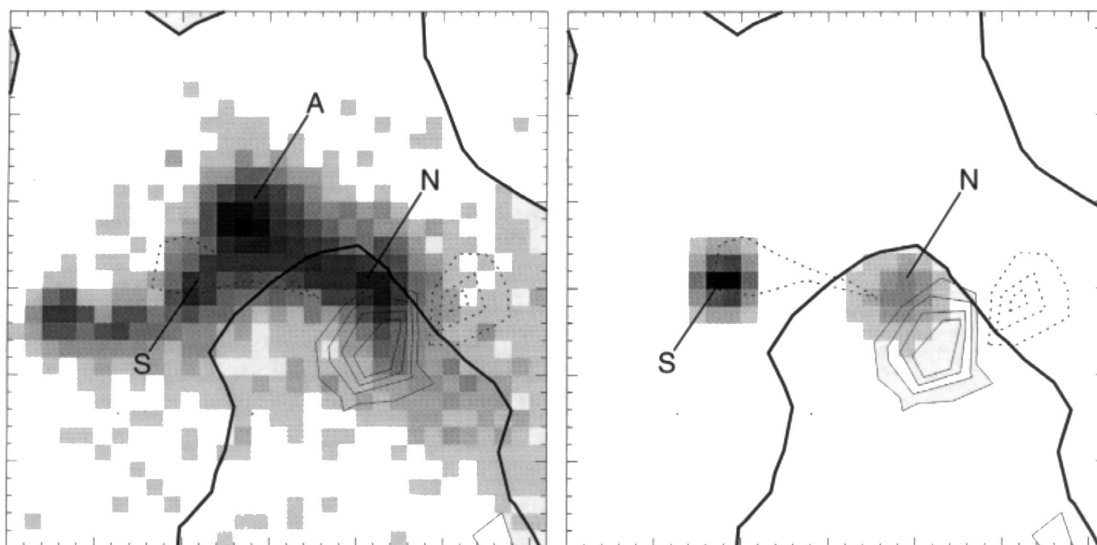


FIG. 6.—1994 August 14 flare. *Left*: SXT image (Al.1 filter, 17:35:07), 31×31 pixels, each $2''.47$ square. *Right*: HXT image (H channel, 17:35:49) during burst P1, integration period 17:35:49.8–17:36:05.8 UT.

TABLE 2
A SUMMARY OF THE HARD X-RAY FLUX, VERTICAL MAGNETIC FIELD, AND ELECTRIC CURRENT DENSITY

Date of Flare	NOAA	Source	Hard X-Ray Intensity ^a	B_z (Gauss)	J_z (σ)
1991 Nov 15.....	6919	N:S	100:55	400:800	<1.5:3
1991 Dec 26.....	6985	N2:S	7.7:1.7	200:400	1.5:3
1992 Aug 20.....	7260	S1:S2:A	2.2:2.5:0.8	200:300:400	<1.5:<1.5:2
1993 Jun 7.....	7518	N:S	10:6	1600:3000	<1.5:<1.5
1993 Jul 4.....	7530	S:N	3.4:...	200:800	<1.5:4.5
1994 Aug 14.....	7765	S:N	16:10	400:800	1.5:6

^a Hard X-ray intensity is from a spatial integration over the hard X-ray footprint. The unit is counts pixel⁻¹ s⁻¹. For comparison among the six flares, all intensities are measured in the M2 channel.

explains this observation. Many nonthermal electrons (of energy appropriate to emission of hard X-rays) precipitating down to the strong-field footpoint are reflected by a magnetic mirror. These reflected electrons bounce back to the weak-field footpoint, where they collide with the dense chromosphere, creating a more intense hard X-ray source there. The added information that our study brings is that the current density is larger near the footpoint with higher magnetic field.

The weaker hard X-ray sources are near, but not cospatial with, sites of high vertical current density in the flares that occurred in AR 6919 (Fig. 1), AR 6985 (Fig. 2), AR 7260 (Fig. 3), AR 7518 (Fig. 4), and AR 7765 (Fig. 6). In the flare in AR 7530 (Fig. 5), it is not possible to locate the conjugate footpoint source in hard X-rays.

Studies of the topology of flares have been made on the basis of morphological arguments, qualitative interpretation of vector magnetograms, and potential-field extrapolation of longitudinal magnetograms. Several such studies have concluded that flares and nonthermal electron acceleration occur on magnetic separatrices and separators (e.g., Machado et al. 1983; Mandrini et al. 1995; Démoulin et al.

1993; Brown et al. 1994; and Bagalá et al. 1995). However, the most relevant studies, the potential-field extrapolations of observed magnetograms, neglect currents, which makes them of questionable value for the active regions discussed in this paper.

It should be noted that our observational result, that hard X-ray sources are near—but not cospatial with—sites of high vertical current density, does not contradict the hypothesis that nonthermal electron acceleration occurs on separatrices or separators. In fact, it seems quite consistent with it, in the following sense. Longcope & Strauss (1994) studied the reconnection of line-tied current systems. They showed that the reconnection of such current systems took place in current sheets between them. The large-scale active-region current systems we observe are analogous to the distributed currents in the Longcope & Strauss (1994) study; current sheets are far too thin to be spatially resolved in our observations. Acceleration of energetic electrons in reconnecting current sheets has long been considered as a candidate mechanism for energetic electron acceleration and has received recent support from the discovery of loop-top hard X-ray sources by Masuda et al. (1994). If the accel-

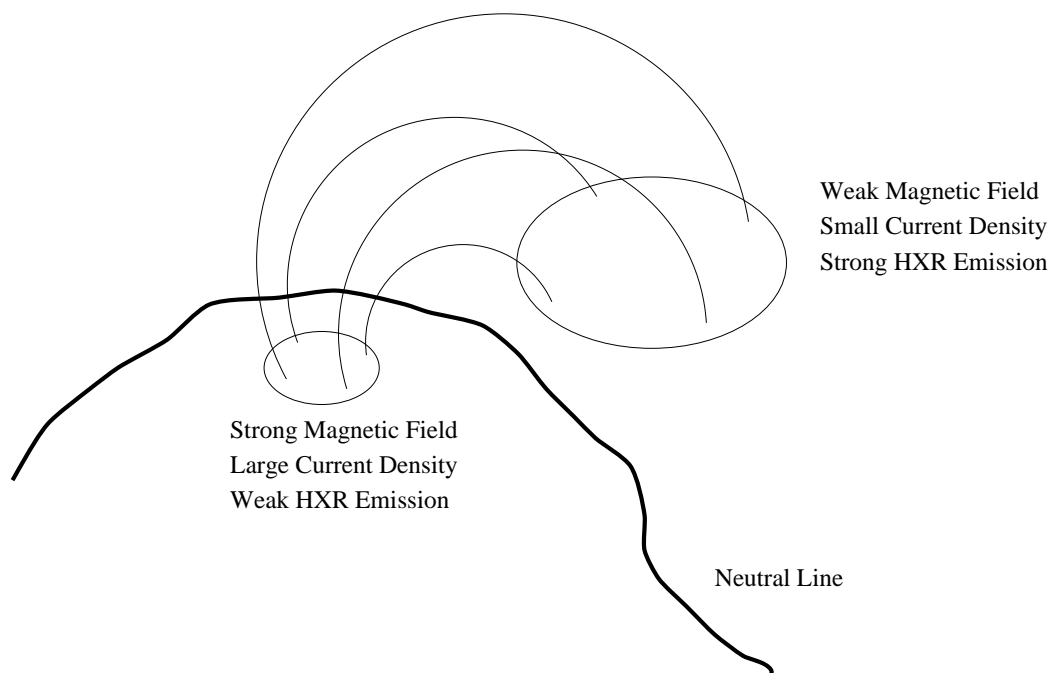


FIG. 7.—“Cornucopia” cartoon

eration of nonthermal electrons takes place in current sheets between current systems in the active regions we have observed, one would expect the observational result we have obtained.

5. CONCLUSIONS

First, we observe that stronger hard X-ray emission in two-footpoint flares occurs at the footpoint having weaker magnetic field and smaller current density. We conclude that this behavior is due to the asymmetry of the magnetic field, as illustrated by the cornucopia model in Figure 7, and the mirroring of the hard X-ray producing nonthermal electrons before they reach the chromosphere.

Second, we have observed several examples in which flare hard X-rays are significantly displaced from maxima in vertical current density. This result, which confirms previous studies that have utilized H α Stark wings as a proxy for the

hard X-rays, leads us to conclude that flare particle acceleration is not a consequence of the interruption of large-scale currents flowing vertically through the photosphere.

We wish to thank Hugh Hudson for initially suggesting the relevance of the cornucopia model to our observations and Dana Longcope for discussions of his results on reconnecting flux tubes. The *Yohkoh* Soft X-Ray Telescope is a collaborative project of the Lockheed Palo Alto Research Laboratory, the National Astronomical Observatory of Japan, and the University of Tokyo, supported by NASA grant NAS8-37334 and ISAS. Mees Solar Observatory is supported by NASA grant NAGW-1542. R. C. C., J. P. W., and T. R. M. were supported through the NASA SXT contract NAS 8-37334 with the Marshall Space Flight Center and the NASA Supporting Research and Technology program.

REFERENCES

- Alfvén, H., & Carlqvist, R. 1967, *Sol. Phys.*, 1, 220
 Bagalá, L. G., Mandrini, C. H., Rovira, M. G., Démoulin, P., & Hénoux, J.-C. 1995, *Sol. Phys.*, 161, 103
 Baum, P. J., & Bratenahl, A. 1980, *Sol. Phys.*, 67, 245
 Brown, J. C. 1971, *Sol. Phys.*, 18, 489
 Brown, J. C., et al. 1994, *Sol. Phys.*, 153, 19
 Canfield, R. C., et al. 1992, *PASJ*, 44, L111
 ———, 1993, *ApJ*, 411, 362
 de La Beaujardière, J.-F., Canfield, R. C., & Leka, K. D. 1993, *ApJ*, 411, 378
 Démoulin, P., Mandrini, C. H., Rovira, M. G., Hénoux, J.-C., & Machado, M. E. 1994, *Sol. Phys.*, 150, 221
 Démoulin, P., van Driel-Gesztelyi, L., Schmieder, B., Hénoux, J.-C., Csepura, G., & Hagyard, M. J. 1994, *A&A*, 271, 292
 Gary, G. A., & Démoulin, P. 1995, *ApJ*, 445, 982
 Gary, G. A., & Hagyard, M. J. 1990, *Sol. Phys.*, 126, 21
 Gorbachev, V. S., & Somov, B. V. 1988, *Sol. Phys.*, 117, 77
 Hagyard, M. J. 1984, in *Proc. Kunming Workshop on Solar Physics and Interplanetary Traveling Phenomena*, Vol. I, ed. C. de Jager & Chen Biao (Kunming: Yunan Observatory), 179
 Hara, H., Tsuneta, S., Acton, L. W., Bruner, M. E., Lemen, J. R., & Ogawara, Y. 1994, *PASJ*, 46, 493
 Hara, H., Tsuneta, S., Lemen, J. R., Acton, L. W., & Mctiernan, J. M. 1992, *PASJ*, 44, L135
 Kosugi, T., Makishima, K., Murakami, T., Sakao, T., Dotani, T., Ogawara, Y., Sawa, M., & Shibasaki, K. 1991, *Sol. Phys.*, 136, 17
 Kosugi, T., Sawa, M., Sakao, T., Masuda, S., Inada-Koide, M., Yaji, K., & Sato, J. 1995, *The Yohkoh HXT Databook October 1991–December 1994*, National Astronomical Observatory, Mitaka, Tokyo, Japan
 Kosugi, T. 1996, in *AIP Conf. Proc. 374, High Energy Solar Physics*, ed. R. Ramaty, N. Mandzhavidze, & X.-M. Hua (New York: AIP), 267
 Leka, K. D., Canfield, R. C., McClymont, A. N., de La Beaujardière, J.-F., Fan, Y., & Tang, F. 1993, *ApJ*, 411, 370
 Leka, K. D., Driel-Gesztelyi, L. V., Nitta, N., Canfield, R. C., Mickey, D. L., Sakurai, T., & Ichimoto, K. 1994, *Sol. Phys.*, 155, 301
 Lin, Y., & Gaizauskas, V. 1987, *Sol. Phys.*, 109, 81
 Longcope, D. W., & Strauss, H. R. 1994, *ApJ*, 437, 851
 Machado, M. E., Somov, B. V., Rovira, M. G., & de Jager, C. 1983, *Sol. Phys.*, 85, 157
 Mandrini, C. H., Démoulin, P., Rovira, M. G., de La Beaujardière, J.-F., & Hénoux, J.-C. 1995, *A&A*, 303, 927
 Masuda, S., Kosugi, T., Hara, H., Sakao, T., Shibata, K., & Tsuneta, S. 1995, *PASJ*, 47, 677
 Masuda, S., Kosugi, T., Hara, H., Tsuneta, S., & Ogawara, Y. 1993, *Nature*, 371, 495
 Metcalf, T. R. 1994, *Sol. Phys.*, 155, 235
 Metcalf, T. R., Hudson, H. S., Kosugi, T., Puetter, R. C., & Pina, R. K. 1996, *ApJ*, 466, 585
 Mickey, D. L. 1985, *Sol. Phys.*, 97, 223
 Moreton, G. E., & Severny, A. B. 1968, *Sol. Phys.*, 3, 282
 Romanov, V. A., & Tsap, T. T. 1990, *Soviet Astron.*, 34, 656
 Sakao, T. 1994, Ph.D. thesis, Univ. Tokyo
 Sakao, T., et al. 1992, *PASJ*, 44, L83
 Smith, D. F., & Priest, E. R. 1972, *ApJ*, 176, 487
 Spicer, D. S. 1981, *Sol. Phys.*, 70, 149
 Tsuneta, S., et al. 1991, *Sol. Phys.*, 136, 37
 Wülser, J.-P., et al. 1994, *ApJ*, 424, 459